

1 High-order cognition is supported by information-rich but
2 compressible brain activity patterns

Lucy L. W. Owen^{1,2} and Jeremy R. Manning^{1,*}

¹Department of Psychological and Brain Sciences,
Dartmouth College, Hanover, NH

²Carney Institute for Brain Sciences,
Brown University, Providence, RI

* Address correspondence to jeremy.r.manning@dartmouth.edu

March 16, 2023

Abstract

We applied dimensionality reduction algorithms and pattern classifiers to functional neuroimaging data collected as participants listened to a story, temporally scrambled versions of the story, or underwent a resting state scanning session. These experimental conditions were intended to require different depths of processing and inspire different levels of cognitive engagement. We considered two primary aspects of the data. First, we treated the maximum achievable decoding accuracy across participants as an indicator of the “informativeness” of the recorded patterns. Second, we treated the number of features (components) required to achieve a threshold decoding accuracy as a proxy for the “compressibility” of the neural patterns (where fewer components indicate greater compression). Overall, we found that the peak decoding accuracy (achievable without restricting the numbers of features) was highest in the intact (unscrambled) story listening condition. However, the number of features required to achieve comparable classification accuracy was also lowest in the intact story listening condition. Taken together, our work suggests that our brain networks flexibly reconfigure according to ongoing task demands, and that the activity patterns associated with higher-order cognition and high engagement are both more informative and more compressible than the activity patterns associated with lower-order tasks and lower levels of engagement.

Keywords: information, compression, temporal decoding, dimensionality reduction, neuroimaging

²⁴ Introduction

25 Large-scale networks, including the human brain, may be conceptualized as occupying one or
26 more positions along on a continuum. At one extreme, every node is fully independent from
27 every other node. At the other extreme, all nodes behave identically. Each extreme optimizes
28 key properties of how the network functions. When every node is independent, the network is

29 maximally *expressive*: if we define the network’s “state” as the activity pattern across its nodes, then
30 every state is equally reachable by a network with fully independent nodes. On the other hand, a
31 network of identically behaved nodes optimizes *robustness*: any subset of nodes may be removed
32 from the network without any loss of function or expressive power, as long as any single node
33 remains. Presumably, most natural systems tend to occupy positions between these extremes. We
34 wondered: might the human brain reconfigure itself to be more flexible or more robust according
35 to ongoing demands? In other words, might the brain reconfigure its connections or behaviors
36 under different circumstances to change its position along this continuum?

37 Closely related to the above notions of expressiveness versus robustness are measures of
38 how much *information* is contained in a given signal or pattern, and how *redundant* a signal
39 is (Shannon, 1948). Formally, information is defined as the amount of uncertainty about a given
40 variables’ outcomes (i.e., entropy), measured in *bits*, or the optimal number of yes/no questions
41 needed to reduce uncertainty about the variable’s outcomes to zero. Highly complex systems with
42 many degrees of freedom (i.e., high flexibility and expressiveness), are more information-rich than
43 simpler or more constrained systems. The redundancy of a signal denotes the difference between
44 how expressive the signal *could* be (i.e., proportional to the number of unique states or symbols
45 used to transmit the signal) and the actual information rate (i.e., the entropy of each individual
46 state or symbol). If a brain network’s nodes are fully independent, then the number of bits required
47 to express a single activity pattern is proportional to the number of nodes. The network would
48 also be minimally redundant, since the status of every node would be needed to fully express a
49 single brain activity pattern. If a brain network’s nodes are fully coupled and identical, then the
50 number of bits required to express a single activity pattern is proportional to the number of unique
51 states or values any individual node can take on. Such a network would be highly redundant,
52 since knowing any individual node’s state would be sufficient to recover the full-brain activity
53 pattern. Highly redundant systems are also robust, since there is little total information loss due
54 to removing any given observation.

55 We take as a given that brain activity is highly flexible: our brains can exhibit nearly infinite
56 varieties of activity patterns. This flexibility implies that our brains activity patterns are highly
57 information rich. However, brain activity patterns are also highly structured. For example,
58 full-brain correlation matrices are stable within (Finn et al., 2017, 2015; Gratton et al., 2018) and

59 across (Cole et al., 2014; Glerean et al., 2012; Gratton et al., 2018; Yeo et al., 2011) individuals. This
60 stability suggests that our brains' activity patterns are at least partially constrained, for example
61 by anatomical, external, or internal factors. Constraints on brain activity that limit its flexibility
62 decrease expressiveness (i.e., its information rate). However, constraints on brain activity also
63 increase its robustness to noise (e.g., "missing" or corrupted signals may be partially recovered).
64 For example, recent work has shown that full-brain activity patterns may be reliably recovered
65 from only a relatively small number of implanted electrodes (Owen et al., 2020; Scangos et al.,
66 2021). This robustness property suggests that the relevant signal (e.g., underlying factors that
67 have some influence over brain activity patterns) are compressible.

68 To the extent that brain activity patterns contain rich task-relevant information, we should
69 be able to use the activity patterns to accurately differentiate between different aspects of the
70 task (e.g., using pattern classifiers; Norman et al., 2006). For example, prior work has shown a direct
71 correspondence between classification accuracy and the information content of a signal (Alvarez,
72 2002). To the extent that brain activity patterns are compressible, we should be able to generate
73 simplified (e.g., lower dimensional) representations of the data while still preserving the relevant
74 or important aspects of the original signal. In general, information content and compressibility are
75 related but are partially dissociable (Fig. 1). If a given signal (e.g., a representation of brain activity
76 patterns) contains more information about ongoing cognitive processes, then the peak decoding
77 accuracy should be high. And if the signal is compressible, a low-dimensional embedding of the
78 signal will be similarly informative to the original signal (Fig. 1D).

79 Several recent studies suggest that the complexity of brain activity is task-dependent, whereby
80 simpler tasks with lower cognitive demands are reflected by simpler and more compressible brain
81 activity patterns, and more complex tasks with higher cognitive demands are reflected by more
82 complex and less compressible brain activity patterns (Mack et al., 2020; Owen et al., 2021). These
83 findings complement other work suggesting that functional connectivity (correlation) patterns are
84 task-dependent (Cole et al., 2014; Finn et al., 2017; Owen et al., 2020), although see Gratton et
85 al. (2018). Higher-order cognitive processing of a common stimulus also appears to drive more
86 stereotyped task-related activity and functional connectivity across individuals (Hasson et al.,
87 2008; Lerner et al., 2011; Simony & Chang, 2020; Simony et al., 2016).

88 The above studies are consistent with two potential descriptions of how cognitive processes are

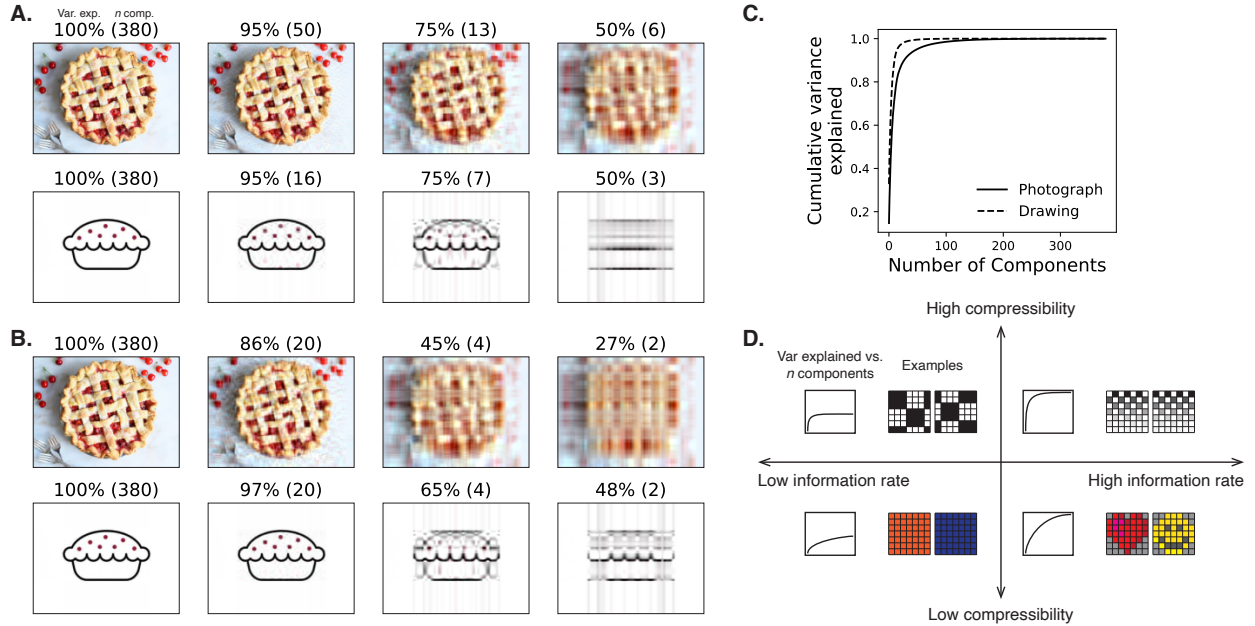


Figure 1: Information content and compressibility. **A. Variance explained for two images.** We applied principal components analysis to a photograph and drawing, treating the rows of the images as “observations.” Across columns, we identified the numbers of components required to explain 100%, 95%, 75%, or 50% of the cumulative variance in each image (the 100% columns denote the original images). The numbers of components are indicated in parentheses, and the resulting “compressed” images are displayed. **B. Representing two images with different numbers of components.** Using the same principal component decompositions as in Panel A, we computed the cumulative proportion of variance explained with 380 (original images), 20, 4, or 2 components. **C. Cumulative variance explained versus number of components.** For the images displayed in Panels A and B, we plot the cumulative proportion of variance explained as a function of the number of components used to represent each image. **D. Information rate and compressibility.** Across multiple images, the information rate (i.e., the amount of information contained in each image; horizontal axis) is high when each individual pixel provides information that cannot be inferred from other pixels. High-information rate images tend to be high-resolution, and low-information rate images tend to be low-resolution. Compressibility is related to the difference between the information required to specify the original versus compressed images (vertical axis). Highly compressible images often contain predictable structure (redundancies) that can be leveraged to represent the images much more efficiently than in their original feature spaces.

89 reflected in brain activity patterns. One possibility is that the information rate of brain activity in-
90 creases during more complex or higher-level cognitive processing. If so, then the ability to reliably
91 decode cognitive states from brain activity patterns should improve with task complexity or with
92 the level (or “depth”) of cognitive processing. A second possibility is that the compressibility of
93 brain activity patterns increases during more complex or higher-level cognitive processing. If so,
94 then individual features of brain recordings, or compressed representations of brain recordings,
95 should carry more information during complex or high-level (versus simple or low-level) cognitive
96 tasks.

97 We used a previously collected neuroimaging dataset to estimate the extent to which each of
98 these two possibilities might hold. The dataset we examined comprised functional magnetic reso-
99 nance imaging (fMRI) data collected as participants listened to an audio recording of a 10-minute
100 story, temporally scrambled recordings of the story, or underwent a resting state scan (Simony
101 et al., 2016). Each of these experimental conditions evokes different depths of cognitive process-
102 ing (Hasson et al., 2008; Lerner et al., 2011; Owen et al., 2021; Simony et al., 2016). We used
103 across-participant classifiers to decode listening times in each condition, as a proxy for how “infor-
104 mative” the task-specific activity patterns were (Simony & Chang, 2020). We also used principle
105 components analysis to generate lower-dimensional representations of the activity patterns. We
106 then repeated the classification analyses after preserving different numbers of components and
107 examined how classification accuracy changed across the different experimental conditions.

108 Results

109 We sought to understand whether higher-level cognition is reflected by more reliable and in-
110 formative brain activity patterns, and how compressibility of brain activity patterns relates to
111 cognitive complexity. We developed a computational framework for systematically assessing the
112 informativeness and compressibility of brain activity patterns recorded under different cognitive
113 circumstances. We used across-participant decoding accuracy (see *Forward inference and decoding*
114 *accuracy*) as a proxy for informativeness. To estimate the compressibility of the brain patterns, we
115 used group principal components analysis (PCA) to project the brain patterns into k -dimensional
116 spaces, for different values of k (see *Hierarchical Topographic Factor Analysis (HTFA)* and *Principal*

117 components analysis (PCA)). For more compressible brain patterns, decoding accuracy should be
118 more robust to small values of k .

119 We analyzed a dataset collected by Simony et al. (2016) that comprised four experimental
120 conditions. These conditions exposed participants to stimuli that systematically varied in cognitive
121 engagement. In the *intact* experimental condition, participants listened to an audio recording of
122 a 10-minute story. In the *paragraph*-scrambled experimental condition, participants listened to a
123 temporally scrambled version of the story, where the paragraphs occurred out of order, but where
124 the same set of paragraphs was presented over the entire listening interval. All participants in
125 this condition experienced the scrambled paragraphs in the same order. In the *word*-scrambled
126 experimental condition, participants listened to a temporally scrambled version of the story, where
127 the words occurred in a random order. Again, all participants in this condition experienced the
128 scrambled words in the same order. Finally, in the *rest* experimental condition, participants lay
129 in the scanner with no overt stimulus, while keeping their eyes open and blinking as needed.
130 This public dataset provided a convenient means for testing our hypothesis that different levels
131 of cognitive processing and engagement affect how informative and compressible the associated
132 brain patterns are.

133 To evaluate the relation between informativeness and compressibility for brain activity from
134 each experimental condition, we trained a series of across-participant temporal decoders on com-
135 pressed representations of the data. Figure 2A displays the decoding accuracy as a function
136 of the number of principal components used to represent the data (also see Fig. S1). Several
137 patterns were revealed by the analysis. First, in general (i.e., across experimental conditions),
138 decoding accuracy tends to improve as the number of components are increased. However, de-
139 coding accuracy peaked at higher levels for experimental conditions that exposed participants
140 to cognitively richer stimuli (Fig. 2D). The peak decoding accuracy was highest for the “intact”
141 condition (versus paragraph: $t(99) = 35.205, p < 0.001$; versus word: $t(99) = 43.172, p < 0.001$);
142 versus rest: $t(99) = 81.361, p < 0.001$), next highest for the “paragraph” condition (versus word:
143 $t(99) = 6.243, p < 0.001$; versus rest: $t(99) = 50.748, p < 0.001$), and next highest for the “word”
144 condition (versus rest: $t(99) = 48.791, p < 0.001$). This ordering implies that cognitively richer
145 conditions evoke more stable brain activity patterns across people.

146 The cognitively richer conditions also displayed steeper initial slopes. For example, the intact

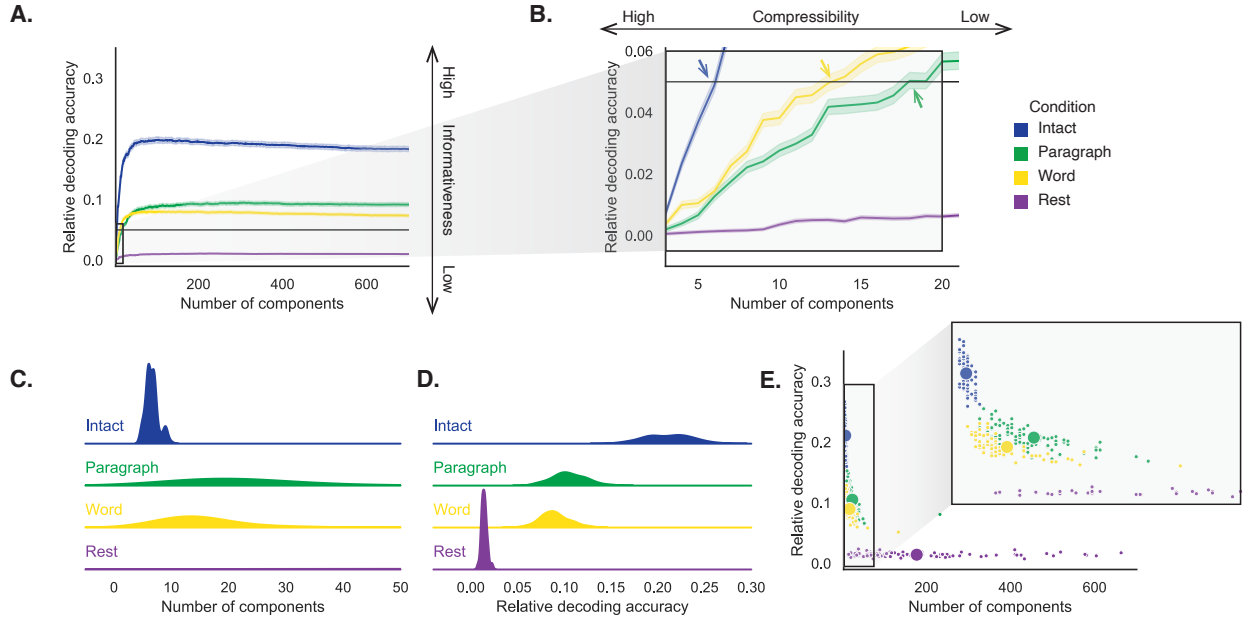


Figure 2: Decoding accuracy and compression. **A. Decoding accuracy by number of components.** Ribbons of each color display cross-validated decoding performance for each condition (intact, paragraph, word, and rest), as a function of the number of components (features) used to represent the data. For each condition, decoding accuracy has been normalized by subtracting expected “chance” decoding performance (estimated as $\frac{1}{T}$, where T is the number of timepoints in the given condition). This normalization was intended to enable fairer comparisons across conditions; a relative decoding accuracy of 0.0 denotes “chance” performance. The horizontal black line denotes 5% decoding accuracy (used as a reference in Panel B). **B. Numbers of components required to reach a fixed decoding accuracy threshold, by condition.** The panel displays a zoomed-in view of the inset in Panel A. Intersections between each condition’s decoding accuracy curve and the 5% decoding accuracy reference line are marked by arrows. All error ribbons in Panels A and B denote bootstrap-estimated 95% confidence intervals. **C. Estimating “compressibility” for each condition.** The density plots display the numbers of components required to reach at least 5% (corrected) decoding accuracy, across all cross validation runs. For the “rest” condition, where decoding accuracy never reached 5% accuracy, we display the distribution of the numbers of components required to achieve the peak decoding accuracy in each fold. (This distribution is nearly flat, as illustrated in Panel E.) **D. Estimating “informativeness” for each condition.** The density plots display the peak (corrected) decoding accuracies achieved in each condition, across all cross validation runs. **E. Informativeness versus compressibility.** Each dot displays the minimum number of components required to achieve at least 5% corrected decoding accuracy (x -coordinate; for the rest condition the numbers of components are estimated using the peak decoding accuracies as in Panel C) and the peak (corrected) decoding accuracy (y -coordinate). The smaller dots correspond to individual cross validation runs and the larger dots display the averages across runs. The inset displays a zoomed-in view of the indicated region in the main panel.

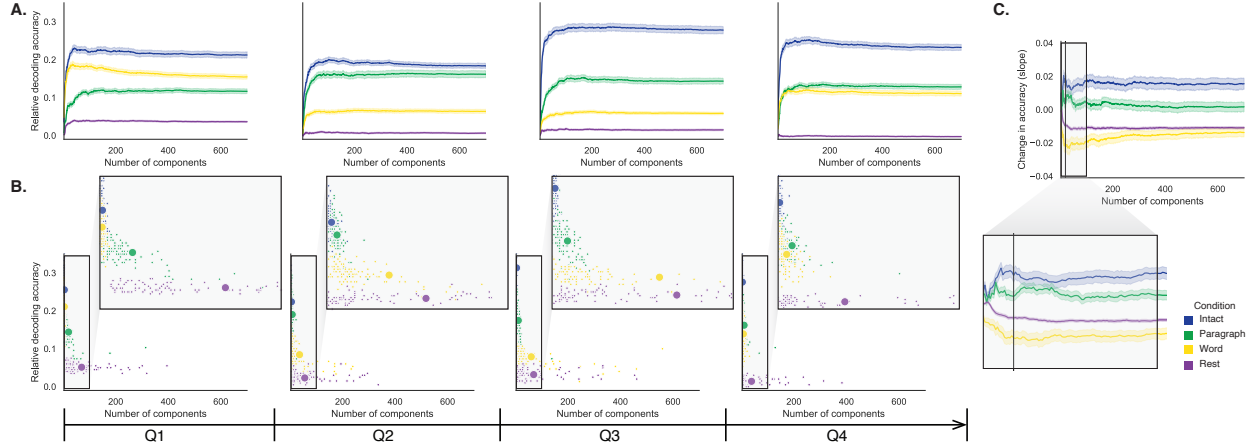


Figure 3: Changes in decoding accuracy and compression over time. **A. Decoding accuracy by number of components, by story segment.** Each family of curves is plotted in the same format as Figure 2A but reflects data only from one quarter of the dataset. **B. Informativeness versus compressibility by condition and segment.** Each scatter plot is in the same format as Figure 2E, but reflects data only from one quarter of the dataset. **C. Change in decoding accuracy over time, by number of components.** For each number of components (x -axis) and condition (color), we fit a regression line to the decoding accuracies obtained for the first, second, third, and fourth quarters of the dataset (corresponding to the columns of Panels A and B). The y -axis denotes the slopes of the regression lines. All error ribbons denote bootstrap-estimated 95% confidence intervals.

147 condition decoders reached an arbitrarily chosen threshold of 5% accuracy using fewer components
 148 than the paragraph condition decoders ($t(99) = -7.429, p < 0.001$) or word condition decoders
 149 ($t(99) = -7.300, p < 0.001$), and decoding accuracy never exceeded 5% for the rest condition. This
 150 suggests that brain activity patterns evoked by cognitively richer conditions are more compressible,
 151 such that representing the data using the same number of principal components provides more
 152 information to the temporal decoders (Figs. 2B, C). Taken together, as shown in Figure 2E, we
 153 found that brain activity patterns evoked by cognitively richer conditions tended to be both more
 154 informative (i.e., associated with higher decoding accuracies) *and* more compressible (i.e., requiring
 155 fewer components to achieve the 5% accuracy threshold).

156 If informativeness (to the temporal decoders) and compressibility vary with the cognitive
 157 richness of the stimulus, might these measures also vary over time *within* a given condition? For
 158 example, participants in the intact condition might process the ongoing story more deeply later
 159 on in the story (compared with earlier in the story) given the additional narrative background
 160 and context they had been exposed to by that point. To examine this possibility, we divided
 161 each condition into four successive time segments. We computed decoding curves (Fig. 3A)

and the numbers of components required to achieve 5% decoding accuracy (Fig. 3B) for each segment and condition. We found that, in the two most cognitively rich conditions (intact and paragraph), both decoding accuracy and compressibility, as reflected by the change in decoding curves, increased with listening time (e.g., at the annotated reference point of $k = 20$ components in Fig. 3C: intact: $t(99) = 7.915, p < 0.001$; paragraph: $t(99) = 2.354, p = 0.021$). These changes may reflect an increase in comprehension or depth of processing with listening time. In contrast, the decoding accuracy and compressibility *decreased* with listening time in the word condition ($t(99) = -10.747, p < 0.001$) and rest condition ($t(99) = -22.081, p < 0.001$). This might reflect the depletion of attentional resources in the less-engaging word and rest conditions.

We also wondered how informativeness and compressibility in the different experimental conditions might vary across brain networks. We used a network parcellation identified by Yeo et al. (2011) to segment the brain into seven distinct networks. The networks can be sorted (roughly) in order from lower-level to higher-level cortex as follows (Figs. 4A–C): visual, somatomotor, dorsal attention, ventral attention, limbic, frontoparietal, and default mode. Next, we computed decoding curves separately for the activity patterns within each network and identified each network's inflection point, for each experimental condition. Moving from low-order networks to higher-order networks, we found that decoding accuracy tended to increase, particularly in the higher-order experimental conditions (Fig. 4D, E). This suggests that higher-order networks may carry more content-relevant or stimulus-driven "information." We found no clear trends in the proportions of components required to achieve 5% decoding accuracy across networks or conditions (Fig. 4F).

In addition to examining different networks in isolation, we wondered about the general structure of the full-brain (i.e., potentially multi-network) activity patterns reflected by different principal components across different experimental conditions. As shown in Figure 5, we used Neurosynth (Rubin et al., 2017) to identify, for each component, the associations with each of 80 themes (see *Reverse inference*). In general, the first principal components across all of the experimental conditions tended to weight most heavily on themes related to cognitive control, memory, language processing, attention, and perception. Other components appeared to vary more across conditions.

To gain further insights into which brain functions might be most closely associated with

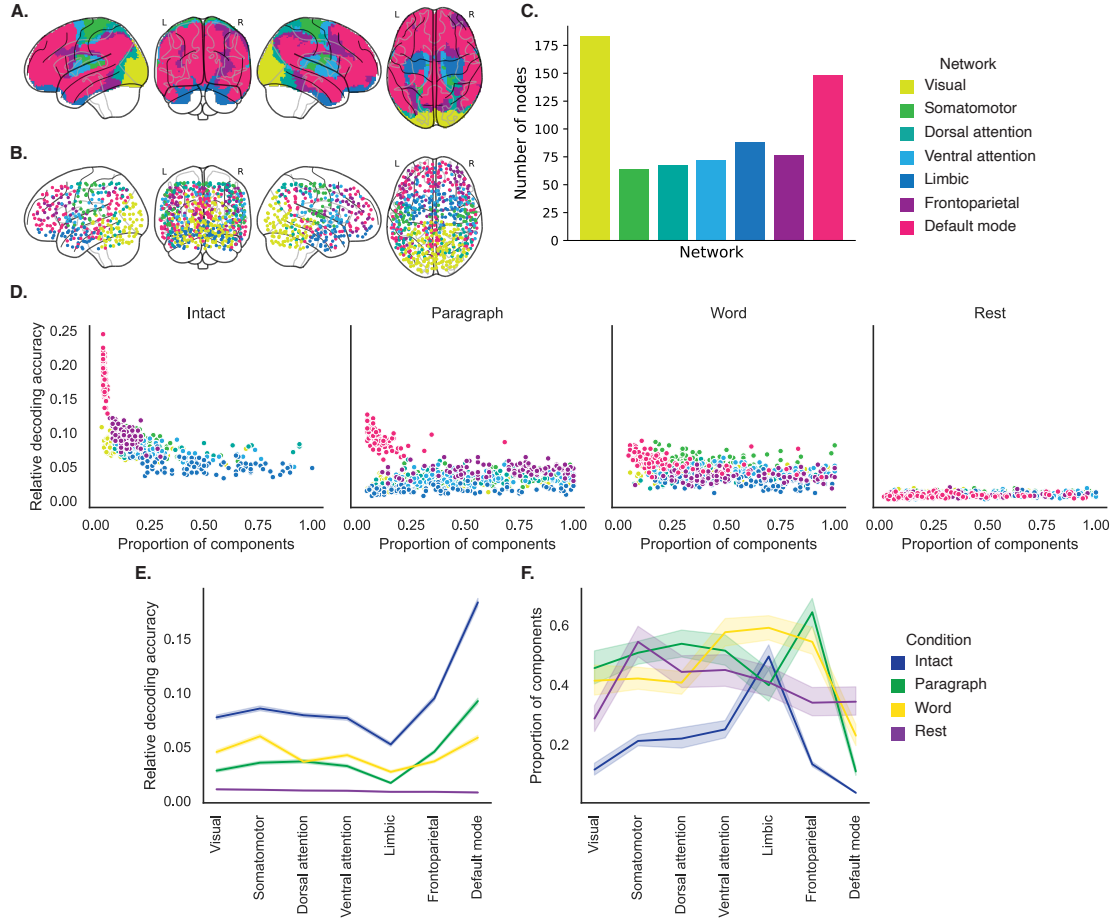


Figure 4: Network-specific decoding accuracy and compression. **A. Network parcellation map.** The glass brain displays the location of each of seven networks identified by Yeo et al. (2011). **B. Node labels.** We assigned network labels to each of 700 Hierarchical Topographic Factor Analysis-derived nodes (see *Hierarchical topographic factor analysis (HTFA)*). For each node, we evaluated its radial basis function (RBF) at the locations of every voxel in the parcellation map displayed in Panel A. We summed up these RBF weights separately for the voxels in each network. We defined each node's network label as its highest-weighted network across all voxels. **C. Per-network node counts.** The bar plot displays the total number of HTFA-derived nodes assigned to each network. **D. Informativeness versus compressibility by network and condition.** Each dot corresponds to a single cross validation run. The dots' coordinates denote the minimum proportion of components (relative to the number of nodes in the given network) required to achieve at least 5% corrected decoding accuracy (x -coordinate; for the rest condition these proportions are estimated using the peak decoding accuracies) and peak (corrected) decoding accuracy (y -coordinate). We repeated the analysis separately for each network (color) and experimental condition (column). **E. Informativeness by network.** For each network, sorted (roughly) from lower-order networks on the left to higher-order networks on the right, the curves display the peak (corrected) decoding accuracy for each experimental condition (color). **F. Compressibility by network.** For each network, the curves display the proportion of components (relative to the total possible number of components displayed in Panel C) required to achieve at least 5% decoding accuracy (or, for the rest condition, peak decoding accuracy, as described above). Error ribbons in Panels E and F denote 95% bootstrap-estimated confidence intervals.

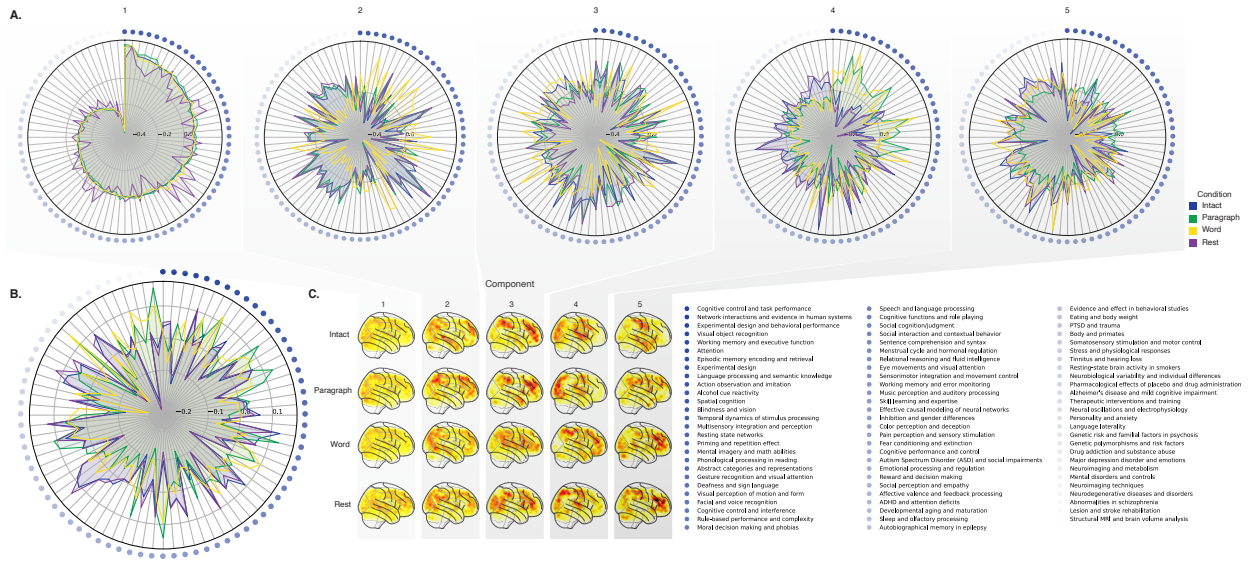


Figure 5: Neurosynth topic weightings by component. We used a reverse inference procedure (see *Reverse inference*) to estimate the correspondences between brain images and a set of 80 topics derived from the Neurosynth database of neuroimaging articles (Rubin et al., 2017). **A. Topic correlations by component.** For each of the top five highest-weighted principal components (columns) derived from each experimental condition (colors), the radar plots display the correlations between the component images and the per-topic images derived for each topic (topic identities are denoted by the blue dots; a legend for the topic labels is in the lower right of the figure). An annotated list of the top-weighted topics for each component and condition may be found in Figure S2 and the top-weighted terms for each topic may be found in Table S1. **B. Topic correlations averaged across components.** The radar plot is in the same format as the plots in Panel A, but here we display the per-condition average correlations across the top five components (for each condition) reflected in Panel A. **C. Component images.** Each plot displays a right sagittal view of a glass brain projection of the top five principal components (columns) for each experimental conditions (rows). Additional projections for each component may be found in Figure S3.

the top-weighted components from each experimental condition, we manually grouped each Neurosynth-derived topic into a smaller set of core cognitive functions. Separately for each component, we computed the average weightings across all topics that were tagged as being associated with each of these cognitive functions (Figs. 6A, S5A). To help visualize these associations, we used the patterns of associations for each component to construct graphs whose nodes were experimental conditions and cognitive functions (Figs. 6B, S5B). We also computed correlations between the sets of per-topic weightings from each of the top-weighted components from each experimental condition (Fig. 6C, D) and between the brain maps for each condition's components (Fig. S5C, D). Taken together, we found that each component appeared to weight on a fundamental set of cognitive functions that varied by experimental condition. For example, the top principal components from every condition weighted similarly on the full set of Neurosynth topics (Fig. 5A) and cognitive functions (Figs. 6A, B and S5 A, B), suggesting that these components might reflect a set of functions or activity patterns that are common across all conditions. The second components' weightings were similar across the intact, paragraph, and rest conditions (highest-weighted functions: cognitive control, memory, social cognition, and resting state), but different for the word condition (highest-weighted functions: sensory perception and cognitive control). The fourth components' weighting were grouped the paragraph and word conditions (highest-weighted functions: memory, language processing, and cognitive control) and the intact and rest conditions (highest-weighted functions: emotion, social cognition). We also used ChatGPT (OpenAI, 2023) to sort the list of manually tagged cognitive functions from lowest-level to highest-level (Tab. S2, Fig. 6E; also see *Ranking cognititive processes*). We found that higher-level functions tended to be weighted on more heavily by top components from the intact and paragraph conditions than lower-level functions. The top components from the word condition showed the opposite tendency, whereby *lower*-level functions tended to be weighted on more heavily than higher-level functions. The components from the rest condition showed almost no differences in the weights associated with high-level versus low-level functions.

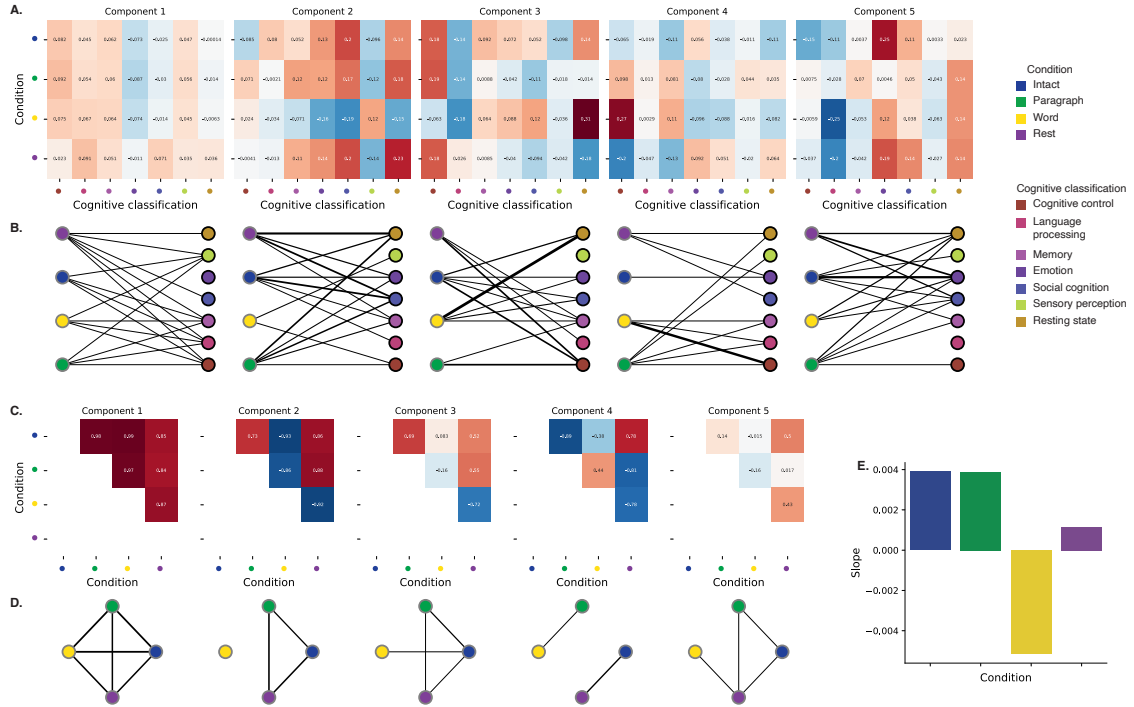


Figure 6: Summary of functions associated with top-weighted components by condition. A. Top-weighted topics by condition. Here we display per-condition (rows, indicated by colored dots) topic correlations, averaged across topics that pertain to each of several broad cognitive functions (columns within each sub-panel, indicated by colored dots). Each sub-panel reflects correlations for the components indicated in the panel titles. A legend for the condition and several core cognitive function classifications is displayed in the lower right of the figure. Table S1 provides a list of each topic's top-weighted terms, along with each topic's manually labeled cognitive classification. A full list of the topics most highly associated with each component may be found in Figure S2. **B. Associations between per-condition components and cognitive functions.** The network plots denote positive average correlations between the component images for each condition (gray-outlined dots on the left sides of each network; colors denote conditions) and topic-specific brain maps associated with each indicated cognitive function (black-outlined dots on the right sides of each network; colors denote cognitive functions). The line thicknesses are proportional to the correlation values (correlation coefficients are noted in the heatmaps in Panel A). **C. Correlations between each principal component, by condition.** The heatmaps display the correlations between the brain maps (Fig. S3) for each principal component (sub-panel), across each pair of conditions (rows and columns of each sub-panel's matrix, indicated by colored dots). **D. Associations between per-condition components, by component.** Each sub-panels network plot summarizes the pattern of correlations between the n^{th} top-weighted principal components (sub-panel) for each experimental condition (gray-outlined dots). The line thicknesses are proportional to the correlation values (correlation coefficients are noted in the heatmaps in Panel C). **E. Change in weights by condition.** The bar heights reflect the slopes of regression lines, fit separately to the top five components from each condition, between the ChatGPT-derived "rank" of each cognitive classification and the correlations between the component and topic maps associated with cognitive processes at the given rank (see *Ranking cognitive processes*). Also see Fig. S5 for additional information.

218 **Discussion**

219 We examined fMRI data collected as participants listened to an auditory recording of a story, scram-
220 bled recordings of the story, or underwent a resting state scan. We found that cognitively richer
221 stimuli evoked more reliable (i.e., consistent across people) and information rich brain activity pat-
222 terns. The brain patterns evoked by cognitively richer stimuli were also more compressible, in that
223 each individual component provided more “signal” to temporal decoders relative to components
224 of data from less cognitively rich conditions (Fig. 2). Over time (e.g., as the experiment progressed),
225 these phenomena were strengthened. Specifically, across story segments, data from more cogni-
226 tively rich conditions became more informative and compressible, and data from less cognitively
227 rich conditions became *less* informative and compressible (Fig. 3). We also repeated these analyses
228 separately for different brain networks. We found that networks traditionally associated with
229 higher-level cognitive functions tended to provide more informative brain patterns than networks
230 traditionally associated with lower level cognitive functions (Fig. 4). Finally, we examined the
231 most dominant components of the brain activity patterns from each experimental condition. We
232 used a reverse inference approach (Rubin et al., 2017) to identify the terms in the neuroimaging
233 literature most commonly associated with the corresponding maps. As summarized in Figure 6,
234 we found that terms associated with memory and sensory processing were associated with the
235 strongest components in all three story listening conditions. Terms associated with sensory in-
236 tegration were associated with the strongest components in the intact and paragraph-scrambled
237 conditions. Terms associated with sentence comprehension, emotion, and valence were associated
238 with the strongest components in the intact condition. Finally, terms associated with the default
239 mode network were associated with the strongest components in the word-scrambled and resting
240 state conditions. Taken together, our findings indicate that the informativeness and compressibil-
241 ity of our brain activity patterns are task-dependent, and these properties change systematically
242 with factors like cognitive richness and depth of processing.

243 Our explorations of informativeness and compressibility are related to a much broader litera-
244 ture on the correlational and causal structure of brain activity patterns (Adachi et al., 2012; Bassett
245 & Sporns, 2017; Brovelli et al., 2004; Bullmore & Sporns, 2009; Dhamala et al., 2008; Korzeniewska
246 et al., 2008; Owen et al., 2021; Preti et al., 2017; Rogers et al., 2007; Rubinov & Sporns, 2010; Size-

more et al., 2018; Smith, Beckmann, et al., 2013; Smith, Vidaurre, et al., 2013; Sporns & Betzel, 2016; Sporns & Honey, 2006; Sporns & Zwi, 2004; Srinivasan et al., 2007; Tomasi & Volkow, 2011; Yeo et al., 2011). Correlations or causal associations between different brain regions simultaneously imply that full-brain activity patterns will be compressible and also that those activity patterns will contain redundancies. For example, the extent of which activity patterns at one brain area can be inferred or predicted from activity patterns at other areas (e.g., Owen et al., 2020; Scangos et al., 2021), reflects overlap in the information available in or represented by those brain areas. If brain patterns in one area are recoverable using brain patterns in another area, then the “signal” used to convey the activity patterns could be compressed by removing the recoverable activity. Predictable (and therefore redundant) brain activity patterns are also more robust to signal corruption. For example, even if the activity patterns at one region are unreadable or unreliable at a given moment, that unreliability could be compensated for by other regions’ activity patterns that were predictive of the unreliable region.

Our findings that informativeness and compressibility change with task demands may follow from task-dependent changes in full-brain correlation patterns. A number of prior studies have found that so-called “functional connectivity” (i.e., correlational) patterns vary reliably across tasks, events, and situations (Cole et al., 2014; Owen et al., 2021; Simony et al., 2016; Smith et al., 2009). By examining how these task-dependent changes in correlations affect informativeness and compressibility, our work suggests a potential reason why the statistical structure of brain activity patterns might vary with cognitive task or with cognitive demands. For lower-level tasks, or for tasks that require relatively little “deep” cognitive processing, our brains may optimize activity patterns for robustness and redundancy over expressiveness, for example to maximize reliability. For higher-level tasks, or for tasks that require deeper cognitive processing, our brains may sacrifice some redundancy in favor of greater expressiveness.

In the information theory sense (Shannon, 1948), when a signal is transmitted using a fixed alphabet of “symbols,” the information rate decreases as the signal is compressed (e.g., fewer symbols transmitted per unit time, using an alphabet with fewer symbols, etc.). Our finding that each individual brain component (symbol) becomes more informative as cognitive richness increases suggests that the “alphabet” of brain activity patterns is also task-dependent. Other work suggests that the representations that are *reflected* by brain activity patterns may also change with task de-

277 mands. For example, our brains may represent the same perceptual stimulus differently depending
278 on which aspects of the stimulus or which combinations of features are task-relevant (Mack et al.,
279 2020).

280 Different brain networks also varied in how informative and compressible their activity pat-
281 terns were across experimental conditions (e.g., Fig. 4). This might follow from evolutionary
282 optimizations that reflect the relevant constraints or demands placed on those networks. One
283 possibility is that cortex is organized in a hierarchy of networks “concerned with” or selective to
284 different levels of processing or function. To the extent that different levels of processing (e.g.,
285 low-level sensory processing versus “deeper” higher-level processing) reflect different stimulus
286 timescales (e.g., Manning, 2020), the network differences we observed might also relate to the
287 timescales at which each network is maximally sensitive (Baldassano et al., 2017; Hasson et al.,
288 2008; Lerner et al., 2011; Regev et al., 2018).

289 **Concluding remarks**

290 Cognitive neuroscientists are still grappling with basic questions about the fundamental “rules”
291 describing how our brains respond, and about how brain activity patterns and the associated
292 underlying cognitive representations and computations are linked. We identified two aspects of
293 brain activity patterns, informativeness and compressibility, that appear to change systematically
294 with task demands and across brain networks. Our work helps to clarify how the “neural code”
295 might be structured, and how the code might vary across tasks and brain areas.

296 **Methods**

297 We measured properties of recorded neuroimaging data under different task conditions that varied
298 systematically in cognitive engagement and depth of processing. We were especially interested in
299 how *informative* and *compressible* the activity patterns were under these different conditions (Fig. 1).

300 **Functional neuroimaging data collected during story listening**

301 We examined an fMRI dataset collected by Simony et al. (2016) that the authors have made publicly
302 available at arks.princeton.edu/ark:/88435/dsp015d86p269k. The dataset comprises neuroimaging

303 data collected as participants listened to an audio recording of a story (intact condition; 36 par-
304 ticipants), listened to temporally scrambled recordings of the same story (17 participants in the
305 paragraph-scrambled condition listened to the paragraphs in a randomized order and 36 in the
306 word-scrambled condition listened to the words in a randomized order), or lay resting with their
307 eyes open in the scanner (rest condition; 36 participants). Full neuroimaging details may be found
308 in the original paper for which the data were collected (Simony et al., 2016). Procedures were
309 approved by the Princeton University Committee on Activities Involving Human Subjects, and by
310 the Western Institutional Review Board (Puyallup, WA). All subjects were native English speakers
311 with normal hearing and provided written informed consent.

312 **Hierarchical topographic factor analysis (HTFA)**

313 Following our prior related work, we used HTFA (Manning et al., 2018) to derive a compact
314 representation of the neuroimaging data. In brief, this approach approximates the timeseries
315 of voxel activations (44,415 voxels) using a much smaller number of radial basis function (RBF)
316 nodes (in this case, 700 nodes, as determined by an optimization procedure; Manning et al., 2018)).
317 This provides a convenient representation for examining full-brain activity patterns and network
318 dynamics. All of the analyses we carried out on the neuroimaging dataset were performed in
319 this lower-dimensional space. In other words, each participant's data matrix was a number-of-
320 timepoints (T) by 700 matrix of HTFA-derived factor weights (where the row and column labels
321 were matched across participants). Code for carrying out HTFA on fMRI data may be found as
322 part of the BrainIAK toolbox (Capota et al., 2017; Kumar et al., 2021), which may be downloaded
323 at brainiak.org.

324 **Principal components analysis (PCA)**

325 We applied group PCA (Smith et al., 2014) separately to the HTFA-derived representations of the
326 data (i.e., factor loadings) from each experimental condition. Specifically, for each condition, we
327 considered the set of all participants' T by 700 factor weight matrices. We used group PCA to project
328 these 700-dimensional matrices into a series of shared k -dimensional spaces, for $k \in \{3, 4, 5, \dots, 700\}$.
329 This yielded a set of number-of-participants matrices, each with T rows and k columns.

330 **Temporal decoding**

331 We sought to identify neural patterns that reflected participants' ongoing cognitive processing of
332 incoming stimulus information. As reviewed by Simony et al. (2016), one way of homing in on
333 these stimulus-driven neural patterns is to compare activity patterns across individuals. In partic-
334 ular, neural patterns will be similar across individuals to the extent that the neural patterns under
335 consideration are stimulus-driven, and to the extent that the corresponding cognitive representa-
336 tions are reflected in similar spatial patterns across people (Simony & Chang, 2020). Following this
337 logic, we used an across-participant temporal decoding test developed by Manning et al. (2018) to
338 assess the degree to which different neural patterns reflected ongoing stimulus-driven cognitive
339 processing across people. The approach entails using a subset of the data to train a classifier to
340 decode stimulus timepoints (i.e., moments in the story participants listened to) from neural pat-
341 terns. We use decoding (forward inference) accuracy on held-out data, from held-out participants,
342 as a proxy for the extent to which the inputted neural patterns reflected stimulus-driven cognitive
343 processing in a similar way across individuals.

344 **Forward inference and decoding accuracy**

345 We used an across-participant correlation-based classifier to decode which stimulus timepoint
346 matched each timepoint's neural pattern. For a given value of k (i.e., number of principal compo-
347 nents), we first used group PCA to project the data from each condition into a shared k -dimensional
348 space. Next, we divided the participants into two groups: a template group, $\mathcal{G}_{\text{template}}$ (i.e., training
349 data), and a to-be-decoded group, $\mathcal{G}_{\text{decode}}$ (i.e., test data). We averaged the projected data within
350 each group to obtain a single T by k matrix for each group. Next, we correlated the rows of the two
351 averaged matrices to form a T by T decoding matrix, Λ . In this way, the rows of Λ reflected time-
352 points from the template group, while the columns reflected timepoints from the to-be-decoded
353 group. We used Λ to assign temporal labels to each timepoint (row) from the test group's ma-
354 trix, using the row of the training group's matrix with which it was most highly correlated. We
355 repeated this decoding procedure, but using $\mathcal{G}_{\text{decode}}$ as the template group and $\mathcal{G}_{\text{template}}$ as the
356 to-be-decoded group. Given the true timepoint labels (for each group), we defined the decoding
357 accuracy as the average proportion of correctly decoded timepoints, across both groups (where

358 chance performance is $\frac{1}{T}$). In Figures 2 and 3 we report the decoding accuracy for each condition
359 and value of k , averaged across $n = 100$ cross validation folds.

360 **Reverse inference**

361 To help interpret the brain activity patterns we found within the contexts of other studies, we
362 created summary maps of each principal component, for each experimental condition. Each
363 principal component comprises 700 “weights” on each of the HTFA-derived RBF nodes (see
364 *Hierarchical Topographic Factor Analysis*). For each node, we evaluated its RBF at the locations of
365 every voxel in the standard 2 mm MNI152 template brain and multiplied the RBF by the node’s
366 weight. The sum of these weighted RBF activation maps provides a full-brain image, in MNI152
367 space, of the given principal component.

368 Next, we considered 80 topics estimated using Latent Dirichlet Allocation (Blei et al., 2003)
369 applied to 9,204 functional neuroimaging articles in the Neurosynth database (Rubin et al., 2017).
370 The topics, as well as associated brain maps identified using Neurosynth, were identified and
371 reported in several prior studies (Chen et al., 2020; Fox et al., 2014; Sul et al., 2017). The topic
372 labels for each topic were generated automatically with the following ChatGPT (chat.openai.com)
373 prompt: “Please help me come up with intuitive labels for topic topics I found by fitting a topic
374 model to thousands of neuroscience and psychology articles. I’ll paste in the top 10 highest-
375 weighted words for each topic, and I’d like you to respond with a suggested label. For each topic,
376 please respond with just the topic label and no other formatting or text. Here are the next topic’s
377 top words:” followed by a comma-separated list of the given topic’s top-weighted words reflected
378 in the Table S1. For some topics, ChatGPT responded with a longer-form response rather than a
379 concise topic label. In these instances, on a case-by-case basis, we used a second follow-up prompt
380 to achieve the given topic’s label: “could you please come up with a more concise label for that
381 topic?”. We then manually identified a set of 11 cognitive labels that were intended to encapsulate
382 a representative range of widely studied low-level and high-level cognitive functions. In choosing
383 the set of cognitive labels, we jointly considered each topic’s ChatGPT-derived topic label, along
384 with the top-weighted words for the topic. We attempted to generate a concise set of labels that
385 still spanned the full set of cognitive functions reflected across the 80 topics. Topics that appeared

386 unrelated to specific cognitive functions (e.g., topics related to specific methods or clinical themes)
387 are designated with dashes in Table S1.

388 Finally, following an approach used in several prior studies (Chen et al., 2020; Fox et al., 2014;
389 Sul et al., 2017) we treated the correlation between a given component's brain map and each
390 topic's brain map as a reflection of how much the component was reflective of the given topic.
391 This resulted in a set of 80 "weights" (correlation coefficients) for each component's brain map,
392 with one weight per Neurosynth-derived topic.

393 **Ranking cognitive processes**

394 We manually identified 11 cognitive labels spanning the set of 80 Neurosynth-derived topics:
395 cognitive control, language processing, memory, emotion, social cognition, spatial cognition, at-
396 tention, reward, sensory perception, motor control, and resting state. We then used ChatGPT
397 to automatically "rank" the processes from high-level to low-level using the following prompt:
398 "Please rank these cognitive processes from highest-level to lowest-level, where higher values
399 indicate higher-order or higher-level processes. return the result as a csv file with a header row
400 and two columns: 'Cognitive label' and 'Rank'. Here are the processes: cognitive control, lan-
401 guage processing, memory, emotion, social cognition, spatial cognition, attention, reward, sensory
402 perception, motor control, resting state". Table S2displays the output. We used these labels
403 in the analysis presented in Figure 6E to help summarize difference in topic weightings across
404 experimental conditions.

405 **Data and code availability**

406 All of the code used to produce the figures and results in this manuscript, along with links to the
407 corresponding data, may be found at github.com/ContextLab/pca_paper.

408 **Acknowledgements**

409 We acknowledge discussions with Rick Betzel, Luke Chang, Emily Finn, and Jim Haxby. Our
410 work was supported in part by NSF CAREER Award Number 2145172 to J.R.M. The content is

411 solely the responsibility of the authors and does not necessarily represent the official views of our
412 supporting organizations. The funders had no role in study design, data collection and analysis,
413 decision to publish, or preparation of the manuscript.

414 Author contributions

415 Conceptualization: J.R.M. and L.L.W.O. Methodology: J.R.M. and L.L.W.O. Implementation: L.L.W.O.
416 Analysis: L.L.W.O. Writing, Reviewing, and Editing: J.R.M. and L.L.W.O. Supervision: J.R.M.

417 References

- 418 Adachi, Y., Osada, T., Sporns, O., Watanabe, T., Matsui, T., Miyamoto, K., & Miyashita, Y.
419 (2012). Functional connectivity between anatomically unconnected areas is shaped by collective
420 network-level effects in the macaque cortex. *Cerebral Cortex*, 22(7), 1586–1592.
- 421 Alvarez, S. A. (2002). *An exact analytical relation among recall, precision, and classification accuracy in*
422 *information retrieval* (Technical Report No. BCCS-02-01). Boston College.
- 423 Baldassano, C., Chen, J., Zadbood, A., Pillow, J. W., Hasson, U., & Norman, K. A. (2017). Discov-
424 ering event structure in continuous narrative perception and memory. *Neuron*, 95(3), 709–721.
- 425 Bassett, D. S., & Sporns, O. (2017). Network neuroscience. *Nature Neuroscience*, 20(3), 353–364.
- 426 Blei, D. M., Ng, A. Y., & Jordan, M. I. (2003). Latent dirichlet allocation. *Journal of Machine Learning*
427 *Research*, 3, 993–1022.
- 428 Brovelli, A., Ding, M., Ledberg, A., Chen, Y., Nakamura, R., & Bressler, S. (2004). Beta oscillations in
429 a large-scale sensorimotor cortical network: directional influences revealed by Granger causality.
430 *Proceedings of the National Academy of Sciences, USA*, 101(26), 9849–9854.
- 431 Bullmore, E., & Sporns, O. (2009). Complex brain networks: graph theoretical analysis of structural
432 and functional systems. *Nature Reviews Neuroscience*, 10(3), 186–198.
- 433 Capota, M., Turek, J., Chen, P.-H., Zhu, X., Manning, J. R., Sundaram, N., ... Shin, Y. S. (2017).
434 *Brain imaging analysis kit*.

- 435 Chen, P.-H. A., Jolly, E., Cheong, J. H., & Chang, L. J. (2020). Intersubject representational
436 similarity analysis reveals individual variations in affective experience when watching erotic
437 movies. *NeuroImage*, 216(116851), doi.org/10.1016/j.neuroimage.2020.116851.
- 438 Cole, M. W., Bassett, D. S., Power, J. D., Braver, T. S., & Petersen, S. E. (2014). Intrinsic and
439 task-evoked network architectures of the human brain. *Neuron*, 83(1), 238–251.
- 440 Dhamala, M., Rangarajan, G., & Ding, M. (2008). Analyzing information flow in brain networks
441 with nonparametric Granger causality. *NeuroImage*, 41(2), 354–362.
- 442 Finn, E. S., Scheinost, D., Finn, D. M., Shen, X., Papademetris, X., & Constable, R. T. (2017).
443 Can brain state be manipulated to emphasize individual differences in functional connectivity.
444 *NeuroImage*, 160, 140–151.
- 445 Finn, E. S., Shen, X., Scheinost, D., Rosenberg, M. D., Huang, J., Chun, M. M., ... Constable, R. T.
446 (2015). Functional connectome fingerprinting: identifying individuals using patterns of brain
447 connectivity. *Nature Neuroscience*, 18, 1664–1671.
- 448 Fox, A. S., Chang, L. J., Gorgolewski, K. J., & Yarkoni, T. (2014). Bridging psychology and
449 genetics using large-scale spatial analysis of neuroimaging and neurogenetic data. *bioRxiv*,
450 doi.org/10.1101/012310.
- 451 Glerean, E., Salmi, J., Lahnakoski, J. M., Jääskeläinen, I. P., & Sams, M. (2012). Functional magnetic
452 resonance imaging phase synchronization as a measure of dynamic functional connectivity.
453 *Brain Connectivity*, 2(2), 91–101.
- 454 Gratton, C., Laumann, T. O., Nielsen, A. N., Greene, D. J., Gordon, E. M., Gilmore, A. W., ...
455 Petersen, S. E. (2018). Functional brain networks are dominated by stable group and individual
456 factors, not cognitive or daily variation. *Neuron*, 98(2), 439–452.
- 457 Hasson, U., Yang, E., Vallines, I., Heeger, D. J., & Rubin, N. (2008). A hierarchy of temporal
458 receptive windows in human cortex. *The Journal of Neuroscience*, 28(10), 2539–2550.
- 459 Korzeniewska, A., Crainiceanu, C. M., Kus, R., Franaszczuk, P. J., & Crone, N. E. (2008). Dynamics
460 of event-related causality in brain electrical activity. *Human Brain Mapping*, 29(10).

- 461 Kumar, M., Anderson, M. J., Antony, J. W., Baldassano, C., Brooks, P. P., Cai, M. B., ... Norman,
462 K. A. (2021). BrainIAK: the brain image analysis kit. *Aperture*, *In press*.
- 463 Lerner, Y., Honey, C. J., Silbert, L. J., & Hasson, U. (2011). Topographic mapping of a hierarchy of
464 temporal receptive windows using a narrated story. *The Journal of Neuroscience*, 31(8), 2906–2915.
- 465 Mack, M. L., Preston, A. R., & Love, B. C. (2020). Ventromedial prefrontal cortex compressesion
466 during concept learning. *Nature Communications*, 11(46), doi.org/10.1038/s41467-019-13930-8.
- 467 Manning, J. R. (2020). Context reinstatement. In M. J. Kahana & A. D. Wagner (Eds.), *Handbook of
468 human memory*. Oxford University Press.
- 469 Manning, J. R., Zhu, X., Willke, T. L., Ranganath, R., Stachenfeld, K., Hasson, U., ... Norman,
470 K. A. (2018). A probabilistic approach to discovering dynamic full-brain functional connectivity
471 patterns. *NeuroImage*, 180, 243–252.
- 472 Norman, K. A., Polyn, S. M., Detre, G. J., & Haxby, J. V. (2006). Beyond mind-reading: multi-voxel
473 pattern analysis of fMRI data. *Trends in Cognitive Sciences*, 10(9), 424–430.
- 474 OpenAI. (2023, March). ChatGPT. Personal communication.
- 475 Owen, L. L. W., Chang, T. H., & Manning, J. R. (2021). High-level cognition during story listening is
476 reflected in high-order dynamic correlations in neural activity patterns. *Nature Communications*,
477 12(5728), doi.org/10.1038/s41467-021-25876-x.
- 478 Owen, L. L. W., Muntianu, T. A., Heusser, A. C., Daly, P., Scangos, K. W., & Manning, J. R. (2020). A
479 Gaussian process model of human electrocorticographic data. *Cerebral Cortex*, 30(10), 5333–5345.
- 480 Preti, M. G., Bolton, T. A. W., & Van De Ville, D. (2017). The dynamic functional connectome:
481 state-of-the-art and perspectives. *NeuroImage*, 160, 41–54.
- 482 Regev, M., Simony, E., Lee, K., Tan, K. M., Chen, J., & Hasson, U. (2018). Propagation of information
483 along the cortical hierarchy as a function of attention while reading and listening to stories.
484 *Cerebral Cortex*.
- 485 Rogers, B. P., Morgan, V. L., Newton, A. T., & Gore, J. C. (2007). Assessing functional connectivity
486 in the human brain by fMRI. *Magnetic Resonance Imaging*, 25(11), 1347–1357.

- 487 Rubin, T. N., Kyojo, O., Gorgolewski, K. J., Jones, M. N., Poldrack, R. A., & Yarkoni, T. (2017).
488 Decoding brain activity using a large-scale probabilistic functional-anatomical atlas of human
489 cognition. *PLoS Computational Biology*, 13(10), e1005649.
- 490 Rubinov, M., & Sporns, O. (2010). Complex network measures of brain connectivity: uses and
491 interpretations. *NeuroImage*, 52, 1059–1069.
- 492 Scangos, K. W., Khambhati, A. N., Daly, P. M., Owen, L. L. W., Manning, J. R., Ambrose, J. B.,
493 ... Chang, E. F. (2021). Biomarkers of depression symptoms defined by direct intracranial
494 neurophysiology. *Frontiers in Human Neuroscience*, In press.
- 495 Shannon, C. E. (1948). A mathematical theory of communication. *Bell System Technical Journal*,
496 27(3), 379–423.
- 497 Simony, E., & Chang, C. (2020). Analysis of stimulus-induced brain dynamics during naturalistic
498 paradigms. *NeuroImage*, 216, 116461.
- 499 Simony, E., Honey, C. J., Chen, J., & Hasson, U. (2016). Dynamic reconfiguration of the default
500 mode network during narrative comprehension. *Nature Communications*, 7(12141), 1–13.
- 501 Sizemore, A. E., Giusti, C., Kahn, A., Vettel, J. M., Betzel, R. F., & Bassett, D. S. (2018). Cliques and
502 cavities in the human connectome. *Journal of Computational Neuroscience*, 44(1), 115–145.
- 503 Smith, S. M., Beckmann, C. F., Andersson, J., Auerbach, E. J., Bijsterbosch, J., Douaud, G., ...
504 Glasser, M. F. (2013). Resting-state fMRI in the Human Connectome Project. *NeuroImage*, 80,
505 144–168.
- 506 Smith, S. M., Fox, P. T., Miller, K. L., Glahn, D. C., Fox, P. M., Mackay, C. E., ... Beckmann,
507 C. F. (2009). Correspondence of the brain's functional architecture during activation and rest.
508 *Proceedings of the National Academy of Sciences, USA*, 106(31), 13040–13045.
- 509 Smith, S. M., Hyvärinen, A., Varoquaux, G., Miller, K. L., & Beckmann, C. F. (2014). Group-PCA
510 for very large fMRI datasets. *NeuroImage*, 101, 738–749.

- 511 Smith, S. M., Vidaurre, D., Beckmann, C. F., Glasser, M. F., Jenkinson, M., Miller, K. L., ... Van
512 Essen, D. C. (2013). Functional connectomics from resting-state fMRI. *Trends in Cognitive Sciences*,
513 17(12), 666–682.
- 514 Sporns, O., & Betzel, R. F. (2016). Modular brain networks. *Annual Review of Psychology*, 67,
515 613–640.
- 516 Sporns, O., & Honey, C. J. (2006). Small worlds inside big brains. *Proceedings of the National Academy
517 of Sciences, USA*, 103(51), 19219–19220.
- 518 Sporns, O., & Zwi, J. D. (2004). The small world of the cerebral cortex. *Neuroinformatics*, 2(2),
519 145–162.
- 520 Srinivasan, R., Winter, W. R., Ding, J., & Nunez, P. L. (2007). EEG and MEG coherence: Measures of
521 functional connectivity at distinct spatial scales of neocortical dynamics. *Journal of Neuroscience
522 Methods*, 166, 41–52.
- 523 Sul, S., Güroğlu, B., Crone, E. A., & Chang, L. J. (2017). Medial prefrontal cortical thinning
524 mediates shifts in other-regarding preferences during adolescence. *Scientific Reports*, 7(8510),
525 doi.org/10.1038/s41598-017-08692-6.
- 526 Tomasi, D., & Volkow, N. D. (2011). Association between functional connectivity hubs and brain
527 networks. *Cerebral Cortex*, 21, 2003–2013.
- 528 Yeo, B. T. T., Krienen, F. M., Sepulcre, J., Sabuncu, M. R., Lashkari, D., Hollinshead, M., ... Buckner,
529 R. L. (2011). The organization of the human cerebral cortex estimated by intrinsic functional
530 connectivity. *Journal of Neurophysiology*, 106(3), 1125–1165.